Synthesis and Applications of Anisotropic Magnetic Iron Oxide Nanoparticles

Lucía Gutiérrez, María del Puerto Morales, and Alejandro G. Roca

1 Introduction

Magnetic iron oxide nanocrystals, i.e. magnetite (Fe_3O_4), maghemite (γ-Fe_2O_3) or any of its intermediate stoichiometries ($Fe_{3-x}O_4$), have been applied in widespread applications since ancient times due to their appealing properties [1]. Being the only iron oxide with Fe ions in two oxidation states (+2, +3), magnetite is an abundant material that can be found in the nature (rocks) together with titanomagnetite [2]. Magnetite nanocrystals can also be found inside some bacteria (magnetotactic bacteria) where it is mineralized in intracellular vesicles, generally 30–100 nm nanocubes surrounded by a membrane and displayed in chains (magnetosomes) [3]. Finally, these nanocrystals can be "artificially" synthesized by top-down methods like high-energy ball milling, crushing or grinding, [4] or "bottom-up" approaches involving colloidal methods like coprecipitation, hydro−/solvothermal and thermal decomposition, rendering better structural properties in terms of crystallinity, purity and solvent solubility [5]. Moreover, magnetite particles in the nanometre range size can be

L. Gutiérrez (✉)
Instituto de Ciencia de Materiales de Aragón, ICMA-CSIC, Universidad de Zaragoza, Zaragoza, Spain

Centro de Investigación Biomédica en Red de Bioingeniería, Biomateriales y Nanomedicina (CIBER-BBN), Madrid, Spain

Department of Analytical Chemistry, Universidad de Zaragoza, Zaragoza, Spain
e-mail: lu@unizar.es

M. P. Morales
Instituto de Ciencia de Materiales de Madrid, ICMM-CSIC, Madrid, Spain

A. G. Roca
MagneticNanostrutures Group, Institut Català de Nanociència i Nanotecnologia, Barcelona, Spain

A. G. Roca et al. (eds.), *Surfaces and Interfaces of Metal Oxide Thin Films, Multilayers, Nanoparticles and Nano-composites*,
https://doi.org/10.1007/978-3-030-74073-3_3

synthesized breaking down the limit of superparamagnetism (random alignment of the magnetic moment in the absence of a magnetic field) leading to very interesting reversible magnetic behaviour that paves the way for new applications.

Magnetite nanocrystals have been used along human history for a wide spectrum of applications. They were used as pigments for ceramics in terracotta pottery since ancient times (ancient Greece) [6] and more recently as pigment for inks, dyes or any other material that required black colour, being the favourite one as magnetite absorbed light much better than other black candidates, and thus, it was more reliable [7]. Then, other application where magnetite nanocrystals were well-established was their use in water purification processes, e.g. heavy metal removal [8]. In the latest decades of the twentieth century, their applicability boosted due to magnetite electronic and magnetic properties at the microscale and nanoscale. Magnetite exhibited a great performance for magnetic recording media, spintronics and biomedicine, in both diagnosis (contrast agents in MRI, magnetic resonance imaging) and therapy (drug delivery vehicles and nanoheaters in magnetic and optical hyperthermia) [9]. For each application, scientists have designed and optimized the material in terms of particle size, shape, aggregation state and internal crystal structure to maximize their performance (Fig. 1).

However, magnetite is not the most stable iron oxide phase and tends to oxidize to maghemite. [10] The oxidation kinetics is faster as the temperature increases, as the atmosphere is richer in oxygen, when particle size drops or the crystallinity is poorer. Magnetic properties, in terms of saturation magnetization and coercivity, decrease after this phase transformation, but not dramatically [11]. Regarding the electrical properties, magnetite is a semimetal due to the electron hoping between the Fe ions of the octahedral sublattice of its structure, while maghemite is an insulator.

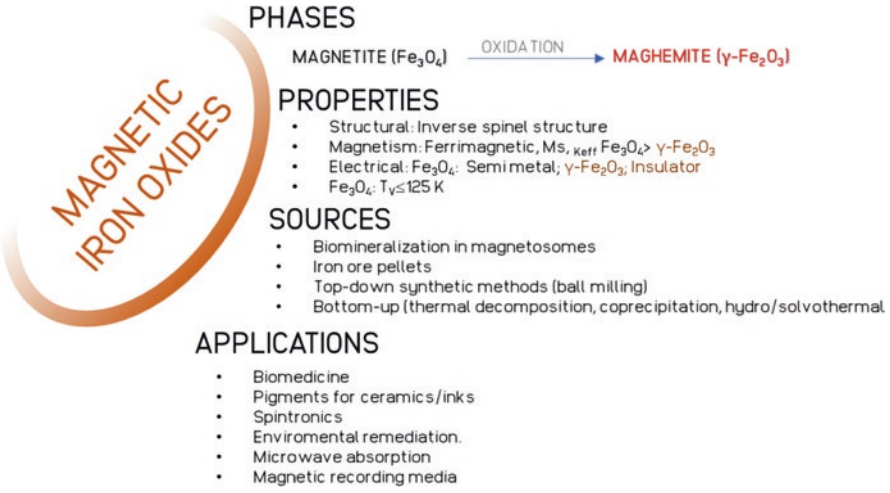

Fig. 1 Schematic description of the most interesting magnetic iron oxide phases, properties, sources and applications that will be considered in this chapter

The aim of this chapter is to present an overview on anisotropic magnetic nanoparticles and their applications in several areas. These nanostructures, with different morphology from the spherical one, have anisotropic properties that depend on the direction of the atoms within the nanostructure and a larger specific surface area. Anisotropic magnetic iron oxide nanoparticles could bring several advantages such as their higher surface-to-volume ratio, enhanced magnetic properties and selected reactivity due to the different facet exposure to the solvent. However, the synthesis of these nanostructures requires the use of different protocols or modification of the established ones. [1]The first section will be focused on the most feasible and successful routes for the preparation of magnetic nanoparticles with a specific morphology. Then, in a second part, we will report the most striking results on the use of these morphologies on diverse applications, ranging from environmental ones to most technological ones, like spintronics or biomedicine. As a summary, magnetite can be considered as an old friend that never gets old fashion and evolves adapting every time to new and more technological applications. This transformation can be understood by its multiple structural, electrical, and magnetic properties and also biodegradability. Thus, with more advanced synthetic techniques, it is possible to tailor the structural properties of magnetite nanocrystals making them an attractive material for the intended application.

2 Preparation of Anisotropic Iron Oxide Nanoparticles

For each application, the concept of "ideal" nanoparticles, i.e. the ones that exhibit the best performance, is different. Therefore, the ideal nanoparticle needs to be tailored mainly by their size and shape. In general, a synthetic route that leads to nanoparticles with an accurate control on their size and shape, low size distribution, aggregation state, high crystallinity and chemical purity is the main goal. The resulting particles would be ideal candidates for the intended applications since all of them will contribute to the desire effect. In this sense, colloidal routes developed in liquid media render nanoparticles accomplishing these properties, with low-cost production and large scalability. Moreover, the obtention of particles in liquid media enables an easier manipulation and postprocessing procedures (e.g. surface modification, deposition forming self-assembly, dispersion in different media).

Magnetite has a cubic cell with an inverse spinel structure (Fd3m) with a cell parameter of 8.394 Å [12]. Fe(II) ions are located in octahedral sites, and Fe(III) ions are located in both octahedral and tetrahedral sites (Fig. 2). The complete oxidation to maghemite keeps the same inverse spinel structure, but all Fe(II) ions are oxidized to Fe(III) and vacancies are created in octahedral positions, distributed coherently [13, 14]. After such transformation, due to the oxidation of the Fe ions, the cell parameter decreases to 8.33–8.35 Å depending on the vacancy order.

The synthesis of anisotropic, i.e. nonspherical, magnetic iron oxide nanoparticles is not trivial (Fig. 3). Thus, structures with hexagonal, orthorhombic or monoclinic crystal symmetry whose facets are perpendicular to the long axis have higher energy

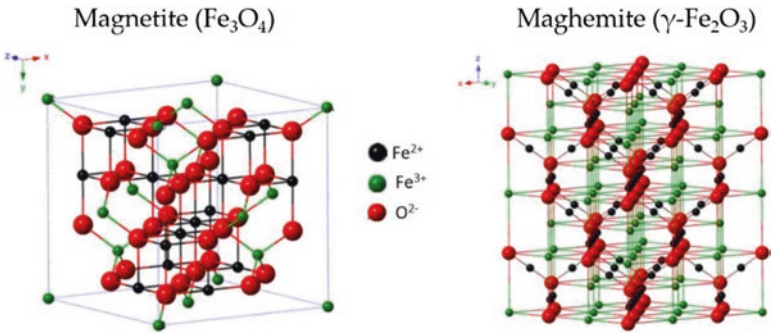

Fig. 2 Crystal structure of magnetite and maghemite. (Adapted with permission from Ref. [15]. © 2015 National Institute for Materials Science)

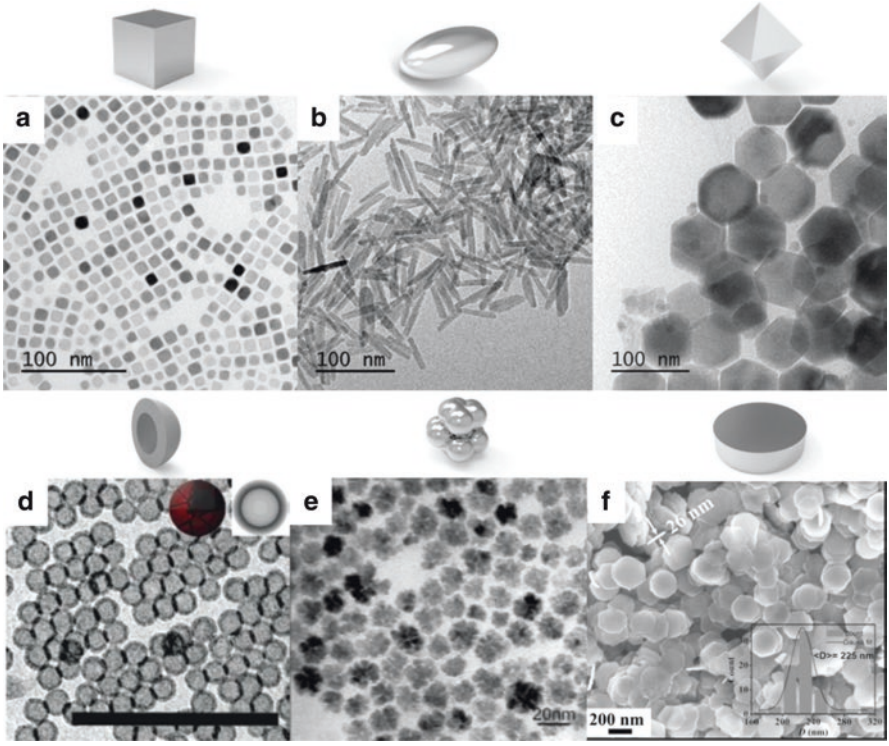

Fig. 3 TEM image of magnetic iron oxide nanoparticles with different morphology: (**a**) nanocubes, (**b**) elongated nanoparticles, (**c**) octahedrons, (**d**) hollow nanoparticles, reprinted with permission from Ref. [31]. Copyright 2007 American Chemical Society; (**e**) nanoflower, reprinted with permission from [32]. Copyright 2017 American Chemical Society. (**f**) SEM image of magnetite nanodiscs. (Adapted with permission from Ref. [33], © 2015, by Wiley)

and lead to elongated structures [16]. However, for cubic crystals, like magnetite, the isotropic growth is favoured. Then, there are two main strategies to induce the growth of anisotropic magnetic iron oxide magnetic nanostructures. The first approach is based on the use of an iron oxide/oxohydroxide as shape template. This strategy consists of two stages where first, an iron oxyhydroxide with the target shape is synthesized (i.e. goethite or akaganeite in elongated nanoparticles) and, in a second step, the oxyhydroxide is reduced to magnetite keeping the desired morphology. The second strategy consists on modifying the reaction kinetics to favour a kinetic regime. In this strategy, there is an essential role played by ligands (molecules or polymers) which bind to metal cations to form intermediate species prior nucleation or to regulate the particle growth through specific adsorption on certain facets of the particle surface. Other key parameters to control the reaction regime are the reaction temperature, the heating rate and the monomer concentration [17, 18].

Magnetite nanocubes could be synthesized in a wide range of sizes, in organic and aqueous media. Using the thermal decomposition in organic media, iron(III) acetylacetonate seems to be the best iron precursor (Fig. 3a). Well-defined ferrimagnetic magnetite nanocubes up to 170 nm can be synthesized using iron (III) acetylacetonate as precursor and oleic acid as surfactant in dibenzyl ether [19]. In this synthesis, the particle size can be modified by changing the iron precursor concentration and reflux time. The addition of a second ligand changes the reaction kinetics and thus decreases the particle size down to 20 nm. Ligands of different nature like decanoic acid, [20] tryoctylphosphine oxide [21], chloride ions [22] or sodium oleate [23] modify the decomposition kinetic and control particles growth by adhering to selective facets of the initial nuclei. Interestingly, a novel strategy using a solvent mixture composed by dibenzyl ether, 1-octadecene and 1-tetradecene with oleic acid and sodium oleate has been reported for the synthesis of more stable and reproducible particles than just using dibenzyl ether [24]. Using this synthesis approach, by increasing the temperature at which the reaction mixture is degassed, Fe_3O_4 nanocubes of 10 nm could be grown. Using an aqueous route, the hydrolysis of iron (II) sulphate in alkaline media mixed with ethanol in the presence of a mild oxidant renders magnetite nanocubes from 30 to 170 nm [25]. This synthesis has been recently scaled up to grams per hour in a continuous flow approach [26].

Magnetite octahedrons exposing the {111} facets are grown through the decomposition of iron (III) oleate in noncoordinating high-boiling point solvents in the presence of an amine or ammonium quaternary salts (Fig. 3c). For example, the decomposition of iron (III) oleate in tetracosane in the presence of oleylamine leads to 21 nm Fe_3O_4 octahedrons [27]. Using trioctylammonium bromide in conjunction with oleic acid as surfactants and squalene as solvent leads to 50 nm Fe_3O_4 octahedrons. [28, 29] Interestingly, the decomposition of iron (0) pentacarbonyl in the presence of a mixture of surfactants and oleylamine/oleic acid 10:1 leads to 50 nm octahedral particles [30].

Elongated or rod-like Fe_3O_4 nanoparticles have been traditionally synthesized using a shape template as intermediate, but nowadays they can also be prepared directly in organic media (Fig. 3b). Due to its crystal structure, hexagonal hematite

(α-Fe_2O_3) [34], orthorhombic goethite (α-Fe_2O_3) [35] or monoclinic akaganeite (β-Fe_2O_3) [36] have been ideal candidates for magnetite templating. In the case of direct synthesis of hematite, the synthesis is very slow (it takes several days) and large nanoparticles (hundreds of nm) are obtained [37]. The concentration of the iron salt, the ageing time and the presence of phosphate ions [37] and urea [38] affect their final length. Interestingly, using akaganeite for templating, the reaction time is reduced and also the particle dimensions [39]. This synthesis could be controlled by modifying the pH but also with the presence of polymers with amine groups, such as polyethylenimine [40, 41]. During the last years, a solvothermal method to grow magnetite nanorods in one step has been developed [42, 43]. This method uses iron (0) pentacarbonyl as precursor in the presence of hexadecylamine and oleic acid, using 1-octanol as solvent. The resulting magnetite rods have lengths from 25 to hundreds of nm and aspect ratios from 5 to 10.

Magnetite discs/plates need the use of an intermediate step for their final synthesis (Fig. 3f). By performing a synthesis where the growth through the long axis is inhibited, it is possible to synthesize hematite disk/plate like nanoparticles that serve as templates. Thus, the use of sodium acetate as inhibitor in the hydrolysis of iron (III) chloride in a mixture of water/ethanol is a robust synthesis route [33, 44, 45]. Then, the reduction could be performed by annealing under inert/reducing atmosphere or in organic media with oleic acid. By this route, it is possible to synthesize discs from 400 x 8 nm to structures of 40 x 40 nm.

Hollow magnetite nanoparticles are obtained through different strategies (Fig. 3d). The sodium resulting from the decomposition of sodium oleate at 380 °C is able to carve iron oxide nanocubes synthesized using iron (III) oleate as precursor [46]. Starting from Fe nanospheres, by passing or generating an oxygen flow through the reaction at high temperatures, the hollowing effect is achieved due to the inward diffusion of oxygen and outward diffusion of the iron cations [31, 47].

Flower-like magnetite nanoparticles, i.e. clusters of magnetite nanoparticles of a controlled size, are mainly synthesized by the polyol method using ethylene glycol as solvent (Fig. 3e). For the cluster formation it is critical the addition of N-methyl diethanolamine, which is used to control the aggregation of the primary cores (5–20 nm) in larger particles of around 30–50 nm [48, 49].

3 Applications

The control of the nanoparticle morphology could bring different benefits such as the enhancement of the magnetic properties due to the shape anisotropy and specific surface area increase in comparison to the spherical morphology. In addition, each morphology exposes different facets of the nanoparticle which determine the final activity of the nanoparticles [50]. All these tuneable properties postulate the anisotropic magnetic iron oxide nanoparticles for widespread applications.

3.1 Biomedicine

Magnetic iron oxide nanoparticles have been widely studied in the biomedical field due to their appealing magnetic properties which can be finely controlled by their size, shape and aggregation state [5, 9]. These particles are biocompatible and biodegradable, since iron is a nutrient and can be metabolized by the organisms [51]. Indeed, iron oxide nanoparticles are the only magnetic material approved by the Food and Drug Administration (FDA) for biomedical applications [52]. Although iron oxide nanoparticles can be biofunctionalized with proteins for specific cell targeting, remarkably, due to their magnetic character, this type of particles can be driven to and accumulated at the desired organ/tissue by magnetic actuation (active targeting) [53]. Magnetic iron oxide nanoparticles can be active agents in both diagnosis and therapy.

Diagnosis

In diagnosis, magnetic iron oxide nanoparticles can be used as T_2 contrast agents in magnetic resonance imaging. This imaging technique is characterized by a high spatial resolution and high soft-tissue contrast. Iron oxide magnetic nanoparticles have a high magnetic moment that produces inhomogeneities in the local magnetic field of the water protons leading to a reduction of the MRI signal intensity on T_2 (transverse relaxation time) weighted images [52]. There were different formulations based on superparamagnetic iron oxide nanoparticles approved by the Food and Drug Administration, but most of them (Feridex, Endorem or Resovist) were removed from the market due to the lack of clinical use [54]. Only Ferumoxytol remains in market due to its low hydrodynamic size (< 40 nm) and its long circulating half-life (15 hours) [55]. To study the capacity of magnetic nanoparticles as contrast agents, one of the variables to study is the longitudinal or transversal relaxivity (r_1 or r_2, respectively), which is a direct measurement of how the magnetic nanoparticles decrease the relaxation time of the water protons due to the perturbation of their magnetic local field.

In general, faceted magnetic iron oxide nanoparticles present better magnetic properties [36, 56] and are more suitable for MRI than their spherical counterparts. Moreover, it seems that a higher specific surface area favours larger r_2 values (Fig. 4). Therefore, **elongated nanoparticles** are particularly a good morphology to be used as MRI contrast agents. Magnetite rods of 25 and 50 nm length (both with 5 nm in diameter) have r_2 values of 670 and 905 $mM^{-1}{\cdot}s^{-1}$, respectively [57]. Thicker magnetite nanorods (70x12 nm), that possess a transversal relaxivity of 608 $mM^{-1}{\cdot}s^{-1}$ and nanorods (30x4 nm) with a r_2 of 312 $mM^{-1}{\cdot}s^{-1}$ [58], also exhibit better performances than the commercial MRI contrast agents (Ferumoxytol; r_2 = 68 $mM^{-1}{\cdot}s^{-1}$).

The exchange interactions given by the clustering of the maghemite particles when they are displayed in **flower-shaped morphology** also brings benefits to their relaxometric properties. 30 nm clusters made of primary units of 10 nm exhibit a r_2

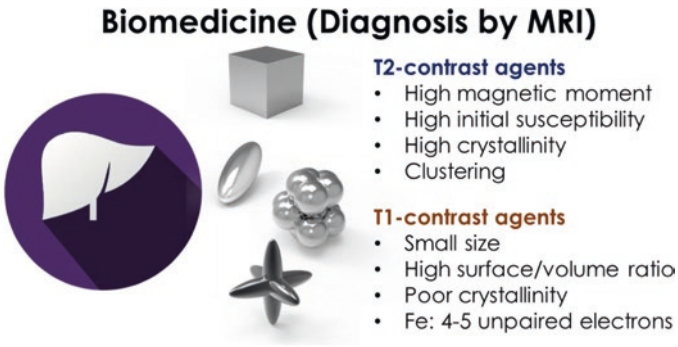

Fig. 4 Magnetic iron oxide morphologies that have shown a better performance for MRI and their fundamental properties

of 365 $mM^{-1}{\cdot}s^{-1}$, near 2 times higher than 10 nm single-core particles made by the same method (polyol). This improvement is due to the cooperative behaviour of the magnetic moment, which increases the intensity of the local magnetic field.

Single 23 nm **magnetite nanocubes** reach a transversal relaxivity value of 398 $mM^{-1}{\cdot}s^{-1}$ [59]. However, it should be noted that the configuration of the nanocubes in solution affects their relaxometric properties as when they are clustered in 200 nm beads, their r_2 decays down to 161 $mM^{-1}{\cdot}s^{-1}$. **Magnetite octopods** of around 30 nm present a considerable high transversal relaxivity value of 679 $mM^{-1}{\cdot}s^{-1}$ (measured at 7 T) much larger than their spherical equivalent (126 $mM^{-1}{\cdot}s^{-1}$) [60].

During the last decade, the research on the use the iron oxides as **T_1 contrast agents** (positive contrast) has been intensified [61, 62]. Magnetic iron oxide nanoparticles with a relatively small size and/or a large surface area increase the exposure of Fe ions to water interface and are ideal candidates for T_1 contrast agents (Fig. 4). Due to its small size, particles tend to be "more paramagnetic" than superparamagnetic exposing their five unpaired Fe^{3+}/Fe^{2+} electrons [62]. Moreover, their longer circulation time and better biocompatibility than gadolinium complexes (the main commercial T_1 contrast agent) postulates iron oxides as a promising material for this application [63]. Also, ultrathin iron oxide nanowhiskers (20x2 nm) have shown interesting properties as T_1 contrast agent with a high r_1 (6.3 $mM^{-1}{\cdot}s^{-1}$) and low r_2 (11.15 $mM^{-1}{\cdot}s^{-1}$) [64], slightly better than 3 nm spherical ultrasmall iron oxide nanoparticles (r_1 = 5.2 $mM^{-1}{\cdot}s^{-1}$; r_2 = 10.4 $mM^{-1}{\cdot}s^{-1}$) [63].

3.2 Therapy

One of the main problems of cancer and other diseases is the difficulty of achieving enough drug concentration at the action site to produce the desired therapeutic effect. Magnetic iron oxide nanoparticles, through two different approaches,

magnetothermia and photothermia, are valuable tools for the design of new and/or more efficient therapies (Fig. 5).

In **magnetic hyperthermia**, magnetic iron oxide nanoparticles can release heat under the application of an alternating magnetic field (50–700 kHz) [65–67]. Since the generated heat affects the tumour locally, it would cause minimal damage to healthy tissues. Therefore, magnetic hyperthermia is an alternative to reduce the side effects of chemotherapy. There are several mechanisms (susceptibility loss, hysteresis losses and viscous heating) by which the magnetic nanoparticles can dissipate heat [68–70]. The particles structural and colloidal properties (i.e. particle size, shape, aggregation state, interactions), the media (viscosity) and the AC field (frequency and amplitude) will determine which of the aforementioned mechanisms is the main one to produce heat. The capability of magnetic nanoparticles to release heat is evaluated by the specific absorption rate (SAR), which can be defined as the power dissipated per unit mass [71].

In the latest years, an intense research has been performed regarding the properties of **magnetite nanocubes for magnetic hyperthermia**. The comparison of nanocubes (19.5 nm) and spheres with the same volume (24 nm) leads to SAR values favourable to the nanocubes. [72] However, comparing heating properties of 53 nm spheres and 43 nm cubes, it was found better heating properties for the spherical ones because the cubes were forming strong and isometric aggregates [73]. Cubes of different sizes (13–38 nm) have been studied finding the best SAR for 19 nm particles 2277 $W \cdot g^{-1}$ (700 kHz, 300 Oe) [74]. Interestingly, the configuration of possible aggregates deeply affects the SAR values. 3D aggregates of 38 nm nanocubes have a SAR of less than 300 $W \cdot g^{-1}$; however, when they were isolated, the SAR increased up to 1400 $W \cdot g^{-1}$ [75]. Nevertheless, it has been demonstrated that the formation of chain-like aggregates aligned in the magnetic field boosts the SAR value by five times compared to 3D aggregates [73]. The measurement of SAR evaluates the possible performance of the nanoparticles; however, when hyperthermia is performed in vivo, it suffers from low heating efficiency due to the high viscosity of the tumour site and particle aggregation upon intracellular internalization

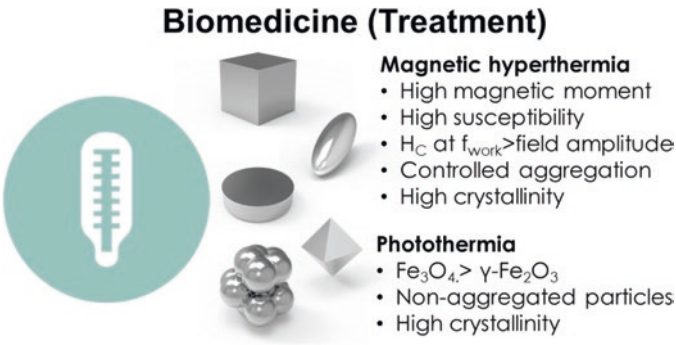

Fig. 5 Magnetic iron oxide morphologies that have shown a better performance for hyperthermia and their fundamental properties

[76]. Thus, the confinement of magnetic nanoparticles in cavities of hundreds of nanometres would enable a certain degree of nanoparticle rotation and minimize aggregation effects, so the heating power would be better preserved intracellularly [77].

Octahedral magnetite nanoparticles have also an optimum morphology to work as nanoheaters in magnetic hyperthermia. Small octahedrons of 6 and 12 nm exhibit SAR values of 163 and 275 $W \cdot g^{-1}$ (247 kHz, 310 Oe) [78]., 40 nm octahedrons reach up to 2483 $W \cdot g^{-1}$ (358 kHz, 800 Oe) and finally 98 nm octahedrons, around the monodomain limit of magnetite, have been reported to reach 2629 $W \cdot g^{-1}$ [79].

Elongated magnetite nanoparticles display moderate heating release properties when compared to other morphologies. The drawback is the high field amplitude needed to obtain a proper heating release due to the high switching field needed to reverse the magnetic moment. Magnetite nanorods grown from the reduction of akaganeite with dimensions of 45x10 nm exhibit a SAR of 1072 $W \cdot g^{-1}$ (390 kHz, 415 Oe), whereas longer rods (400x40 nm) displayed lower SAR values. High crystalline rods made by solvothermal approach exhibit SAR values of 1300 $W \cdot g^{-1}$ (310 kHz, 800 Oe). In contrast, smaller rods of 41x7nm only reached 540 $W \cdot g^{-1}$ [43].

Magnetite nanoplates of certain dimensions have the advantage of the formation of magnetic vortex configurations where spins are arranged circularly and oriented parallel to the field [80]. As a consequence, these particles display negligible coercivity and remanent magnetization which results in extraordinary SAR values, up to 4400 $W \cdot g^{-1}$ for nanoplates of 225 nm in diameter and 26 nm in thickness [81]. However, for nanodiscs without vortex configuration (150–200x10–15 nm), only values of 245 $W \cdot g^{-1}$ (180 kHz, 12 Oe) have been described [44].

Superparamagnetic γ-Fe_2O_3 nanoflowers of 50 nm containing spherical 11 nm particles grown by the polyol method can reach a SAR value of 1790 $W \cdot g^{-1}$, much larger than SAR of single 11 nm (48 $W \cdot g^{-1}$) [49]. Controlled aggregation seems to boost the increase of SAR; however, a compromise between colloidal stability and heating performance should be achieved. In addition to that, nanoparticle cell affinity needs to be maximized through conjugation with biological targeting molecules to increase nanoparticle concentration inside the cells [82].

During the last 5 years, magnetic iron oxides, especially magnetite, have also shown good photothermal properties allowing their use in **photothermal therapy**. Magnetite presents some absorption in the near-infrared range (NIR), especially in the first biological window where water or other biomolecules do not present absorption. The combination of magnetic hyperthermia (900 kHz, 250 Oe) with phototherapy (λ_{las} = 808 nm, 2.5 $W \cdot cm^{-2}$) using 20 nm aggregated magnetite nanocubes resulted in a combined SAR value of 4850 $W \cdot g^{-1}$. Interestingly, by doing just magnetic hyperthermia, a much smaller SAR value (1000 $W \cdot g^{-1}$) was achieved [83–85].

Interestingly, some anisotropic structures could lead to **magnetomechanical actuation** by applying an AC magnetic field of low frequency, just to promote the rotation of the particles. It has been reported that Fe_3O_4 nanorods (200x50 nm) [86] induce cancer cell death on HeLa cells through mechanical oscillations under the

exposure of a 35 kHz field, associated with the Brownian motion of the nanorods [87]. Nanodiscs could also induce cell death through magnetomechanical effects. Nanodiscs made of Permalloy coated with gold (1000x60 nm) were able to exert mechanical forces to N10 glioma cells leading to apoptosis. The AC field of low frequency (60 Hz) induced a shift of the vortex structure, creating an oscillation which was then transmitted to a mechanical force applied to the cell [88]. This strategy opens a new pathway where magnetic iron oxide nanodiscs could be applied.

3.3 Magnetic Recording Media

In the second half of the twentieth century, magnetic recording media were based on acicular iron oxide magnetic nanoparticles (γ-Fe_2O_3) with a length size between 100 and 500 nm and aspect ratios from 6 to 10. They were used as magnetic recording material because of their chemical stability, high magnetic moment aligned with the largest dimension of the particle and high Curie temperature (590–675 °C) to keep moderate coercivity (not too high to allow successful writing and not too small to resist changes or degradation of signals) (Fig. 6) [89, 90]. Elongated morphology was preferred as shape anisotropy is the main contributor to the effective anisotropy, being up to two orders of magnitude higher than the magnetocrystalline one for particles with axial ratio larger than 6. On the other side, the microstructure of the particles, including defects, pores and inhomogeneities, were shown to decrease the effective anisotropy [91, 92]. These problems were inherent to the synthetic routes employed for the growth the magnetic iron oxides using lepidocrocite (γ-FeOOH) or goethite (α-FeOOH) as shape templates, as the subsequent dehydration was the main cause of pore and defects formation [93, 94]. An alternative route was based on the hydrothermal treatment of $Fe(OH)_3$ which leads to hematite (α-Fe_2O_3) bypassing the formation of iron oxyhydroxides and the formation of pores [34, 95]. In the last decade of the twentieth century, iron oxides, as well as chromium dioxide particles, were replaced by metal particulate materials, which possess twice the magnetization of iron oxides and higher coercivity [96–98].

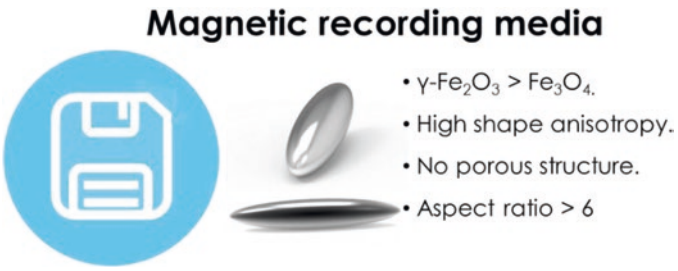

Fig. 6 Magnetic iron oxide morphology tested for magnetic recording media and their fundamental properties

3.4 Water Treatment

One of the major challenges in the environmental field is water treatment for the removal of heavy metal ions like As, Pb, Hg, Cr, Cd and Ni, which cause harmful effects on humans and animals [8]. Moreover, organic pollutants such as detergents and pesticides, all of them from human source, can also be found in water and represent another type of environmental threats. They mainly consist in chlorinated and nonchlorinated aliphatic and aromatic molecules [99]. Traditional methods for water treatment include centrifugation, coagulation, filtration and reverse osmosis. The use of **iron oxide nanoparticles for water remediation** as absorbents of metal ions presents several advantages such as their relatively low cost, the efficient recovery of the material by a simple magnetic separation procedure and also its high specific surface area (Fig. 7) [100]. It has been demonstrated that the absorption capacity of As(III) and As(V) increases from 0.6 to 59.5 mg As·g^{-1} as the magnetite particle size decreases from 300 to 11 nm. These differences were explained by the distinct exposed surface area and the different reactivity of the surfaces (decrease of tetrahedral site occupancy) [101–103]. The main mechanism related to the absorption of pollutants at the particles surface is the complexation and/or electrostatic interaction, followed by ion exchange between the iron surface and the toxic ions [104, 105]. The performance of the iron oxide nanoparticles depends on the crystalline structure (Fe_3O_4 or γ-Fe_2O_3), the particle concentration, the surface coating and the presence of interfering ions (especially nitrate and phosphate ions) [106, 107].

Due to its porous 3D morphology and high specific surface area, **micron-sized nanoflowers** have shown great potential in the absorption of As(V) and Cr(VI). Depending on the phase, values for the absorption of As(V) of 4.65 and 4.75 mg·g^{-1} have been found for Fe_3O_4 and γ-Fe_2O_3, respectively, while smaller differences have been found for the absorption of Cr(VI) (4.38 and 3.86 mg·g^{-1} for Fe_3O_4 and γ-Fe_2O_3) [108]. These nanoflowers have been also tested for the absorption of Orange II reaching absorption values around 43.5 mg·g^{-1}. **Hollow iron oxide nanocubes** with a length of 7 nm and a shell thickness of around 2 nm have shown a powerful capacity for the absorption of As(V) (326 mg·g^{-1}) and As(III) (190 mg·g^{-1})

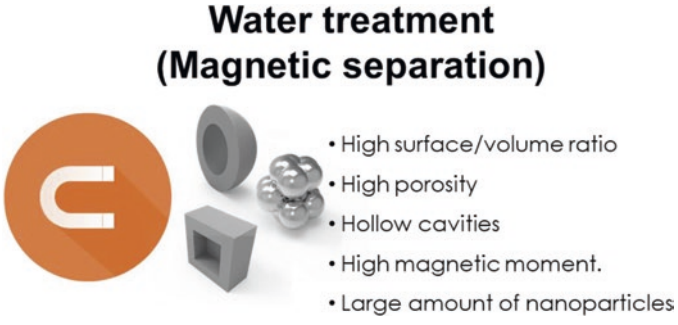

Fig. 7 Magnetic iron oxide morphologies that have shown a better performance for water treatment and their fundamental properties

[109]. **Hollow spheres** between 200 and 300 nm in diameter and 20 nm shell thickness were tested for the absorption and removal of Neutral Red dye reaching values up to 90 $mg \cdot g^{-1}$ [110].

Despite these encouraging results, magnetic nanoparticles have important limitations in their use for water remediation, mainly related to the large quantities required for this application and the difficulties to fulfil the regulations for obtaining drinking water [8, 111].

3.5 Spintronics

Magnetite is a high-valuable material for application in spintronics because it is classified as a half-metallic ferromagnet (bandgap of 0.1–0.15 eV) with high values of spin polarization but also favourable Curie temperature (T_C = 850 K) [112]. Density functional theory (DFT) has predicted a value of −100% spin polarization at the Fermi level for the bulk material [113].

Recently, if has been observed that **8 nm magnetite octahedrons** capped with oleylamine exhibit interesting results in tunnelling magnetoresistance (TMR). [114] The oleylamine surface layer between the particles acts as insulating barrier providing multiple tunnel injection junctions where intergranular tunnelling is possible. TMR at room temperature reaches 38% increasing up to 69% at 180 K, much higher than those measured for spherical 8 nm particles coated with oleylamine (24% at room temperature and 41% at 180 K). The better performance of octahedral particles is a consequence of their better stoichiometry at the surface, presenting less defects that increase the spin polarization of the material and so the TMR. Moreover, the fact that (111) facets are exposed facilitates the strong coupling of oleylamine molecules on them (Fig. 8). **Magnetite nanorods** (75 × 9 nm, aspect ratio 8.3) were also tested as potential material for spintronics, and it was measured a TMR of 14% at room temperature when they were randomly oriented [115]. However, once they were oriented, they could increase its TMR up to 19% and to 31% at 130 K (close to the Verwey transition) because the relative magnetization is maximized due to the parallel orientation of the nanorods. The study of the particle dimensions with the

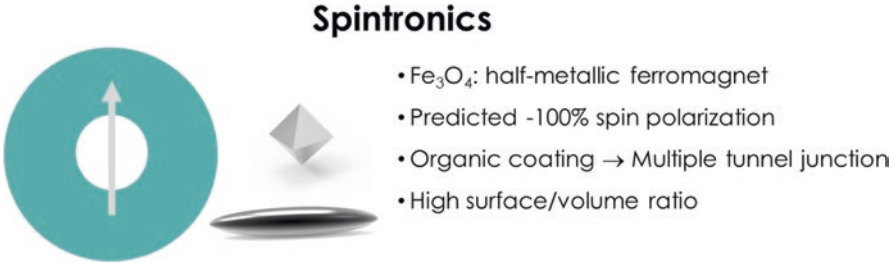

Fig. 8 Magnetic iron oxide morphologies that have shown a better performance for spintronics and their fundamental properties

TMR leads to a TMR decreases with the nanorod dimension, mainly for the diameter. Thus, the spin polarization of the 75 x 9 nm magnetite rods was 46%.

3.6 Microwave Absorption

In recent years, there has been an upsurge of electronic devices and communications (i.e. smartphones, satellite broadcasting, local area network (LAN), radars, etc.) operating in the gigahertz range (GHz) whose main drawback is the electromagnetic noise leading to poorer communications. Moreover, microwave radiation induces a considerable amount of health threats to organisms causing the breakdown of DNA strands, increasing heart rate, weakening the immune response and inducing cancer [116]. In this regard, **iron oxide magnetic nanoparticles** have shown high microwave absorption and low reflection over a broad frequency range. Tuning the particles microwave absorption properties is possible by controlling their size and shape and consequently their magnetic properties, that is high saturation magnetization values and low coercivity that favour larger permeability (Fig. 9) [117]. The development of Fe_3O_4 composites with large anisotropy may exceed the Snoeck limit, having high permittivity and reaching better MW absorption properties [118, 119].

Fe_3O_4 nanodiscs with a thickness of 30 nm have shown an increase of the permittivity with the diameter (from 80 to 500 nm) and resonance frequency [120]. However, the permeability shows an opposite trend (2.0 for the 80 nm and 1.8 for 500 nm discs at 0.1 GHz) due to the increase in shape anisotropy as the diameter grows. The smallest nanodiscs (30x 80 nm) exhibit a high microwave absorption as a consequence of its lower permittivity (RL < -10 dB) with a wide frequency bandwidth of about 2–18 GHz, with a sheet thickness of around 2.1 mm. In the same way, nanorods of Fe_3O_4/Fe/SiO_2 of 1 μm x 80 nm present properties as microwave absorbers since the reflection loss below −10 dB is up to 6.96 GHz with a sheet thickness of 2 mm [121]. Porous magnetite **flowers** with a diameter of 2.5 μm

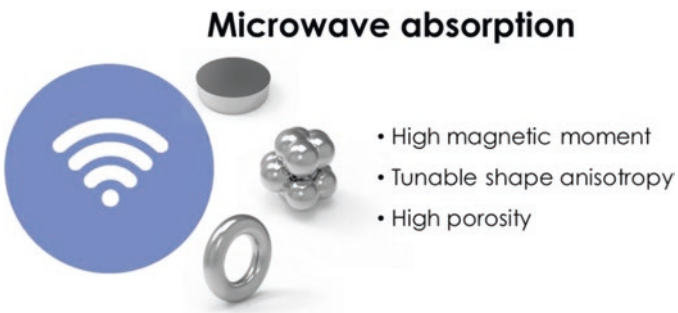

Fig. 9 Magnetic iron oxide morphologies that have shown a better performance for microwave absorption and their fundamental properties

composed of cores of 50 nm present a bandwidth with a RL < -10 dB of 3.8 GHz with a minimum of −28.31 dB at 13.26 GHz. Magnetite **nanorings** coated by carbon of 160 x 70 nm exhibit a strong reflection loss value of 61.54 dB at 16.9 GHz with a thickness of 1.5 mm and a low filling ratio of 25%. Authors attribute this attenuation ability to the eddy current loss enhanced by combination of confinement vortex and train-driven vortex [122].

It can be concluded that the performance of Fe_3O_4 for microwave absorption may require a high anisotropic material that also contains certain porosity in its structure increasing the interfacial area throughout the composite [123].

3.7 Li-Ion Batteries

The use of Fe_3O_4 as material for the design of Li-ion batteries (LIBs) is due to its high theoretical capacity (900–1000 $mA{\cdot}h{\cdot}g^{-1}$), low cost, environmental-friendly and high rate performance [124, 125]. The current generation of LIBs are based on electrode materials in which Li^+ ions are stored by insertion between structural layers during charging and extracted from the layers during discharging without significant structural change, which gives excellent cycling performance. The electrochemical reaction between Li and magnetite occurs as follows:

$$Fe_3O_4 + 8Li^+ + 8e^- \rightarrow 3Fe^0 + 4Li_2O$$

Fe_3O_4 presents several drawbacks for their application as LIBs such as stress due to volume changes after lithium ions charge and discharge and the high surface area of nanomaterials which causes aggregation of the iron oxide nanoparticles and electrolyte decomposition forming a thick solid electrolyte interphase on the electrode surface [126, 127]. Fortunately, the use of high porous and/or hollow nanostructures with high surface area has shown good properties as LIBs materials because they shorten the diffusion pathway of Li ions and electrons and increase the electrochemical reaction area leading to an improvement penetration of the electrolyte and accommodating the strain caused by the lithium inclusion/removal (Fig. 10).

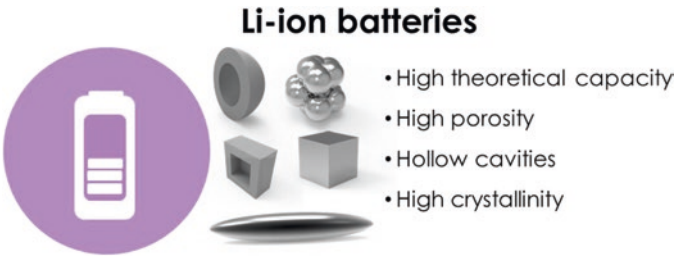

Fig. 10 Magnetic iron oxide morphologies that have shown a better performance for Li-ion batteries and their fundamental properties

For example, high porous **Fe_3O_4 nanorods** with lengths within 400 and 700 nm and diameters between 20 and 80 nm coming from the reduction of goethite nanorods exhibit a high reversible capacity of 843.5 mA·h·g-1 after the 50th cycle at 0.1 C (10 h discharge time) due to the high dense porous structure and the elongated morphology [128]. A composite of **Fe_3O_4 nanoflowers** in carbon with a diameter of 2 μm and sheets of 50 nm in thickness exhibits high capacities up to 1030 mA·h·g^{-1} at a density rate of 0.2 C (5 h discharge time) up to 150 cycles [129]. Noteworthy, it has been observed a different electrochemical activity in the facets exposed to the media by the Fe_3O_4 nanostructures. Thus, (220) facets which can be found in nanoprisms are more electroactive than (111) which are characteristic of octahedrons. [130] Moreover, comparing nanorods, nanoplates and spherical particles, the nanorods present a higher electrochemical activity and larger working capacities [42].

Hollow γ-Fe_2O_3 nanoparticles with a void around 15 nm and a shell thickness near 4 nm can host lithium ions serving as cathode material reaching a capacity of 219 mA·h·g^{-1} with a Coulombic efficiency of 99.7% [131]. In the case of smaller hollow particles (5.7 nm in void with less than 2 nm in shell thickness) capacities up to 132 mA·h·g^{-1} were displayed, being the high concentration of vacancies and chemical stability of γ-Fe_2O_3 during the voltage window the reasons for these high capacity values. On the other hand, **16 nm Fe_3O_4 nanocubes** synthesized by a L-serine-assisted solvothermal approach presents a high specific capacitance of 695 mA·h·g^{-1} at 0.2 C and an excellent Coulombic efficiency of above 95% after the 11th cycle [132]. **Rhombic dodecahedral Fe_3O_4 nanocrystals** (NCs) exposing {110} facets exhibit a high initial discharge capacity of 1147 mA·h·g^{-1} at 0.2 C and a good cycle performance (362 mA·h·g^{-1} at 0.2 C after 100 cycles and 191 mA·h·g^{-1} at 1 C up to 130 cycles) [133].

4 Conclusions and Perspectives

Since ancient times, magnetic iron oxide nanoparticles have been present in people's daily life being remarkable the feasibility of this material to adapt thank to their appealing properties. The possibility of synthesizing these particles using versatile synthetic routes boosted the interest of researchers to establish a clear relation between the electrical, magnetic and optical properties and their particle size, shape and internal structure. It can be concluded that their performance is intimately related to the followed synthetic pathway.

During the latest years, the synthesis of anisotropic magnetic iron oxide nanoparticles, i.e. nanoparticles with nonspherical shape, has received a great attention. The anisometry leads to new functionalities such as enhanced magnetic properties due to the increase in the magnetic effective anisotropy, a higher surface to volume ratio and different particle facets exposed modulating the reactivity with molecules, particles or other entities. These properties are very advantageous in widespread applications such as biomedicine as theranostic agents (MRI and magnetic/optical

hyperthermia) and others such as magnetic recording media, environmental remediation, Li-ion batteries, spintronics or microwave absorption.

This chapter summarizes the most reproducible and successful synthetic routes that lead to iron oxide magnetic nanoparticles with nonspherical morphology and also their applications related to the actual societal challenges. Most of the morphologies considered can be synthesized by thermal decomposition and solvothermal synthesis. Although thermal decomposition produces monodisperse and highly crystalline nanoparticles, this strategy also uses organic solvents which are not environmentally friendly, and for some applications, a further step to transfer them to water is needed. On the other side, solvothermal synthesis produces nanoparticles stable in aqueous media, with less sophisticated protocols and more environmentally friendly solvents. However, this synthesis route is more difficult of scaling up and requires longer time and in many cases a final step for the reduction of the resulting nanoparticles, from hematite to magnetite. Summing up, among the different synthesis routes described here, factors like time, cost, energy consumption, environmental issues and scalability should be considered when translating these processes to the industry.

The applications reviewed in this chapter are very broad, from environmental remediation and biomedicine to spintronics and energy (Li-ion batteries). Most of the research on magnetic nanoparticles for these applications (except magnetic recording media) has been carried out with spherical particles, whose properties depend on particle size, aggregation, crystallinity and coating. However, during the latest decades of the twentieth century, iron oxide and iron metal particles with elongated morphology were the ideal structure for magnetic recording media due to the enhancement of the anisotropy constant. In the latest years, the literature regarding anisometric iron oxides nanoparticles has boosted, demonstrating the interest in them with other areas respect to their spherical equivalents. For example, the use of magnetic nanocubes and nanodiscs in magnetic hyperthermia leads to an increment in the SAR values, also showing a great performance in in vitro studies. Interestingly, the performance of these particles as heating agents can be increased if magnetic hyperthermia is combined with photothermal therapy. On the other hand, nanostructures with high specific surface area that exhibits porosity are very advantageous for Li-ion batteries because they shorten the pathway of Li ions and electrons leading to an improvement penetration of the electrolyte.

In general, the excellent properties of magnetite and maghemite confer these materials of a unique adaptability setting this material far away of being “old fashion” for practical applications. In the case of magnetite, these properties are based on its structure of inverse spinel with an interesting electron hoping between Fe^{2+} and Fe^{3+} ions at octahedral sites. This material has been subject of interest in diverse fields such as magnetism, optics and electronics. Interestingly, most of its properties abruptly change when crossing the Verwey transition. Enabling more degrees of freedom by shaping the morphology of the nanoparticles different from the spherical one has brought advantageous benefits in different applications. For most of the applications, only a few morphologies have been tested yet. There are still morphologies with enormous potential such as plates, rings and nanotubes due to their

magnetic structure (vortex) or specific surface area that have not been tested properly in a variety of applications. Moreover, for some morphologies, there is room to improve the synthetic routes. These routes should be more robust, reproducible and scalable in order to make monodispersed particles with tuneable properties. Moreover, for the demanding application, there should exist more protocols about how to process the material to exhibit the best performance without losing any of its inherent properties.

Acknowledgements This work was supported by the European Commission Framework Programme 7 (NanoMag project, No. 604448). We acknowledge the Spanish Ministry of Economy and Competitiveness through MAT2016-77391, MAT2017-88148-R, RTI2018-095495-J-I00 and PGC2018-096016-B-I00 grants, and Consejo Superior de Investigaciones Científicas through PIE201960E062 project. L.G. acknowledges financial support from the Ramón y Cajal subprogramme (RYC-2014-15512). A.G.R. thanks the Generalitat de Catalunya through 2017-SGR-292 project and the financial support of Ramon Areces Foundation through project CIVP19A5922. The ICN2 is funded by the CERCA programme/Generalitat de Catalunya. The ICN2 is supported by the Severo Ochoa Centres of Excellence programme, funded by the Spanish Research Agency (AEI, grant no. SEV-2017-0706).

References

1. A.G. Roca, L. Gutiérrez, H. Gavilán, et al., Design strategies for shape-controlled magnetic iron oxide nanoparticles. Adv. Drug Deliv. Rev. **138**, 68–104 (2019). https://doi.org/10.1016/j.addr.2018.12.008
2. D.J. Dunlop, Ö. Özdemir, *Rock Magnetism: Fundamentals and Frontiers* (Cambridge University Press, Cambridge, 1997)
3. D. Faivre, D. Schüler, Magnetotactic Bacteria and Magnetosomes. Chem. Rev. **108**, 4875–4898 (2008). https://doi.org/10.1021/cr078258w
4. G. Priyadarshana, N. Kottegoda, A. Senaratne, et al., Synthesis of magnetite nanoparticles by top-down approach from a high purity ore. J. Nanomater. **2015**, 1–8 (2015). https://doi.org/10.1155/2015/317312
5. A.G. Roca, R. Costo, A.F. Rebolledo, et al., Progress in the preparation of magnetic nanoparticles for applications in biomedicine. J Phys D-Applied Phys **42**, 224002 (2009). https://doi.org/10.1088/0022-3727/42/22/224002
6. J. Van Klinken, Magnetization of ancient ceramics. Archaeometry **43**, 49–57 (2001). https://doi.org/10.1111/1475-4754.00004
7. K.J. Sreeram, R. Indumathy, A. Rajaram, et al., Template synthesis of highly crystalline and monodisperse iron oxide pigments of nanosize. Mater. Res. Bull. **41**, 1875–1881 (2006). https://doi.org/10.1016/j.materresbull.2006.03.017
8. K. Simeonidis, S. Mourdikoudis, E. Kaprara, et al., Inorganic engineered nanoparticles in drinking water treatment: A critical review. Environ Sci Water Res Technol **2**, 43–70 (2016). https://doi.org/10.1039/C5EW00152H
9. M. Colombo, S. Carregal-Romero, M.F. Casula, et al., Biological applications of magnetic nanoparticles. Chem. Soc. Rev. **41**, 4306 (2012). https://doi.org/10.1039/c2cs15337h
10. A.G. Roca, J.F. Marco, M.P. Morales, C.J. Serna, Effect of nature and particle size on properties of uniform magnetite and Maghemite nanoparticles. J. Phys. Chem. C **111**, 18577–18584 (2007). https://doi.org/10.1021/jp075133m
11. B.D. Cullity, C.D. Graham, *Introduction to Magnetic Materials* (Wiley, Hoboken, 2008)

12. M.E. Fleet, The structure of magnetite. Acta Crystallogr Sect B Struct Crystallogr Cryst Chem **37**, 917–920 (1981). https://doi.org/10.1107/S0567740881004597
13. M.P. Morales, C. de Julián, J.M. González, C.J. Serna, The effect of the distribution of vacancies on the magnetic properties of γ – Fe2O3 particles. J. Mater. Res. **9**, 135–141 (1994). https://doi.org/10.1557/JMR.1994.0135
14. K.V.P.M. Shafi, A. Ulman, A. Dyal, et al., Magnetic enhancement of γ-Fe_2O_3 nanoparticles by Sonochemical coating. Chem. Mater. **14**, 1778 (2002). https://doi.org/10.1021/cm011535+
15. W. Wu, Z. Wu, T. Yu, et al., Recent progress on magnetic iron oxide nanoparticles: Synthesis, surface functional strategies and biomedical applications. Sci. Technol. Adv. Mater. **16**, 023501 (2015). https://doi.org/10.1088/1468-6996/16/2/023501
16. S.G. Kwon, T. Hyeon, Colloidal chemical synthesis and formation kinetics of uniformly sized Nanocrystals of metals, oxides, and Chalcogenides. Acc. Chem. Res. **41**, 1696–1709 (2008). https://doi.org/10.1021/ar8000537
17. L. Manna, E.C. Scher, A.P. Alivisatos, Synthesis of soluble and processable rod-, arrow-, teardrop-, and tetrapod-shaped CdSe nanocrystals. J. Am. Chem. Soc. **122**, 12700–12706 (2000). https://doi.org/10.1021/ja003055+
18. Z.A. Peng, X. Peng, Mechanisms of the shape evolution of CdSe Nanocrystals. J. Am. Chem. Soc. **123**, 1389–1395 (2001). https://doi.org/10.1021/ja0027766
19. D. Kim, N. Lee, M. Park, et al., Synthesis of uniform Ferrimagnetic magnetite Nanocubes. J. Am. Chem. Soc. **131**, 454–455 (2009). https://doi.org/10.1021/ja8086906
20. P. Guardia, J. Pérez-Juste, A. Labarta, et al., Heating rate influence on the synthesis of iron oxide nanoparticles : The case of decanoic acid. Chem. Commun. **46**, 6108–6110 (2010). https://doi.org/10.1039/c0cc01179g
21. G. Gao, X. Liu, R. Shi, et al., Shape-controlled synthesis and magnetic properties of Monodisperse Fe 3 O 4 Nanocubes. Cryst. Growth Des. **10**, 2888–2894 (2010). https://doi.org/10.1021/cg900920q
22. Z. Xu, C. Shen, Y. Tian, et al., Organic phase synthesis of monodisperse iron oxide nanocrystals using iron chloride as precursor. Nanoscale **2**, 1027 (2010). https://doi.org/10.1039/b9nr00400a
23. M.V. Kovalenko, M.I. Bodnarchuk, R.T. Lechner, et al., Fatty acid salts as stabilizers in size- and shape-controlled Nanocrystal synthesis: The case of inverse spinel Iron oxide. J. Am. Chem. Soc. **129**, 6352–6353 (2007). https://doi.org/10.1021/ja0692478
24. J. Muro-Cruces, A.G. Roca, A. López-Ortega, et al., Precise size control of the growth of Fe 3 O 4 Nanocubes over a wide size range using a rationally designed one-pot synthesis. ACS Nano **13**, 7716–7728 (2019). https://doi.org/10.1021/acsnano.9b01281
25. M. Andrés Vergés, R. Costo, A.G. Roca, et al., Uniform and water stable magnetite nanoparticles with diameters around the monodomain–multidomain limit. J. Phys. D. Appl. Phys. **41**, 134003 (2008). https://doi.org/10.1088/0022-3727/41/13/134003
26. T. Asimakidou, A. Makridis, S. Veintemillas-Verdaguer, et al., Continuous production of magnetic iron oxide nanocrystals by oxidative precipitation. Chem. Eng. J. **393**, 124593 (2020). https://doi.org/10.1016/j.cej.2020.124593
27. L. Zhang, J. Wu, H. Liao, et al., Octahedral Fe_3O_4 nanoparticles and their assembled structures. Chem Commun 4378. (2009). https://doi.org/10.1039/b906636e
28. Shavel A, Rodri B, Pacifico J, et al (2009) Shape Control in Iron Oxide Nanocrystal Synthesis , Induced by Trioctylammonium Ions Shape Control in Iron Oxide Nanocrystal Synthesis , Induced by Trioctylammonium Ions. 5843–5849. https://doi.org/10.1021/cm803201p
29. A. Shavel, L.M. Liz-Marzán, Shape control of iron oxide nanoparticles. Phys. Chem. Chem. Phys. **11**, 3762–3763 (2009). https://doi.org/10.1039/b822733k
30. J. Cheon, N.-J. Kang, S.-M. Lee, et al., Shape evolution of single-crystalline Iron oxide Nanocrystals. J. Am. Chem. Soc. **126**, 1950–1951 (2004). https://doi.org/10.1021/ja038722o
31. A. Cabot, V.F. Puntes, E. Shevchenko, et al., Vacancy coalescence during oxidation of Iron nanoparticles. J. Am. Chem. Soc. **129**, 10358–10360 (2007). https://doi.org/10.1021/ja072574a

32. G. Hemery, A.C. Keyes, E. Garaio, et al., Tuning sizes, morphologies, and magnetic properties of Monocore versus multicore Iron oxide nanoparticles through the controlled addition of water in the Polyol synthesis. Inorg. Chem. **56**, 8232–8243 (2017). https://doi.org/10.1021/acs.inorgchem.7b00956
33. Y. Yang, X. Liu, Y. Lv, et al., Orientation mediated enhancement on magnetic hyperthermia of Fe 3 O 4 Nanodisc. Adv. Funct. Mater. **25**, 812–820 (2015). https://doi.org/10.1002/adfm.201402764
34. M.P. Morales, C. Pecharroman, T. Gonzalez-Carreño, C.J. Serna, Structural characteristics of uniform γ-Fe2O3 particles with different axial (length/width) ratios. J. Solid State Chem. **108**, 158–163 (1994)
35. A.F. Rebolledo, O. Bomatí-Miguel, J.F. Marco, P. Tartaj, A facile synthetic route for the preparation of superparamagnetic iron oxide nanorods and nanorices with tunable surface functionality. Adv. Mater. **20**, 1760–1765 (2008). https://doi.org/10.1002/adma.200701782
36. M.A. Blesa, M. Mijalchik, M. Villegas, G. Rigotti, Transformation of akaganeite into magnetite in aqueous hydrazine suspensions. React Solids **2**, 85–94 (1986). https://doi.org/10.1016/0168-7336(86)80066-3
37. M.P. Morales, T. González-Carreño, C.J. Serna, The formation of alpha-Fe2O 3 monodispersed particles in solution. J. Mater. Res. **7**, 2538–2545 (1992). https://doi.org/10.1557/JMR.1992.2538
38. M. Ocaña, M.P. Morales, C.J. Serna, Homogeneous precipitation of uniform α-Fe_2O_3 particles from Iron salts solutions in the presence of urea. J. Colloid Interface Sci. **212**, 317–323 (1999). https://doi.org/10.1006/jcis.1998.6042
39. O. Bomati-Miguel, A.F. Rebolledo, P. Tartaj, Controlled formation of porous magnetic nanorods via a liquid/liquid solvothermal method. Chem Commun (Camb), 4168–4170 (2008). https://doi.org/10.1039/b805239e
40. S. Lentijo Mozo, E. Zuddas, A. Casu, A. Falqui, Synthesizing Iron oxide nanostructures: The Polyethylenenemine (PEI) role. Crystals **7**, 22 (2017). https://doi.org/10.3390/cryst7010022
41. M. Mohapatra, S. Anand, Synthesis and applications of nano-structured iron oxides / hydroxides – A review. Int. J. Eng. Sci. Technol. **2**, 127–146 (2010). https://doi.org/10.4314/ijest.v2i8.63846
42. H. Sun, B. Chen, X. Jiao, et al., Solvothermal synthesis of Tunable Electroactive magnetite Nanorods by controlling the side reaction. J. Phys. Chem. C **116**, 5476–5481 (2012). https://doi.org/10.1021/jp211986a
43. R. Das, J. Alonso, Z. Nemati Porshokouh, et al., Tunable high aspect ratio Iron oxide Nanorods for enhanced hyperthermia. J. Phys. Chem. C **120**, 10086–10093 (2016). https://doi.org/10.1021/acs.jpcc.6b02006
44. X.-L. Liu, Y. Yang, J.-P. Wu, et al., Novel magnetic vortex nanorings/nanodiscs: Synthesis and theranostic applications. Chinese Phys B **24**, 127505 (2015). https://doi.org/10.1088/1674-1056/24/12/127505
45. Y. Huang, D. Ding, M. Zhu, et al., Facile synthesis of α-Fe 2 O 3 nanodisk with superior photocatalytic performance and mechanism insight. Sci. Technol. Adv. Mater. **16**, 014801 (2015). https://doi.org/10.1088/1468-6996/16/1/014801
46. K. An, T. Hyeon, Synthesis and biomedical applications of hollow nanostructures. Nano Today **4**, 359–373 (2009). https://doi.org/10.1016/j.nantod.2009.06.013
47. A. Cabot, A.P. Alivisatos, V.F. Puntes, et al., Magnetic domains and surface effects in hollow maghemite nanoparticles. Phys. Rev. B **79**, 094419 (2009). https://doi.org/10.1103/PhysRevB.79.094419
48. L. Lartigue, P. Hugounenq, D. Alloyeau, et al., Cooperative Organization in Iron Oxide Multi-Core Nanoparticles Potentiates Their Efficiency as heating mediators and MRI contrast agents. ACS Nano **6**, 10935–10949 (2012). https://doi.org/10.1021/nn304477s
49. P. Hugounenq, M. Levy, D. Alloyeau, et al., Iron oxide Monocrystalline Nanoflowers for highly efficient magnetic hyperthermia. J. Phys. Chem. C **116**, 15702–15712 (2012). https://doi.org/10.1021/jp3025478

50. J. Liu, Z. Wu, Q. Tian, et al., Shape-controlled iron oxide nanocrystals: Synthesis, magnetic properties and energy conversion applications. CrystEngComm **18**, 6303–6326 (2016). https://doi.org/10.1039/C6CE01307D
51. R. Crichton, *Inorganic Biochemistry of Iron Metabolism* (Wiley, Chichester, 2001)
52. A.S. Thakor, J.V. Jokerst, P. Ghanouni, et al., Clinically approved nanoparticle imaging agents. J. Nucl. Med. **57**, 1833–1837 (2016). https://doi.org/10.2967/jnumed.116.181362
53. M. Angelakeris, Magnetic nanoparticles: A multifunctional vehicle for modern theranostics. Biochim Biophys Acta - Gen Subj **1861**, 1642–1651 (2017). https://doi.org/10.1016/j.bbagen.2017.02.022
54. R. Weissleder, M. Nahrendorf, M.J. Pittet, Imaging macrophages with nanoparticles. Nat. Mater. **13**, 125–138 (2014). https://doi.org/10.1038/nmat3780
55. G.B. Toth, C.G. Varallyay, A. Horvath, et al., Current and potential imaging applications of ferumoxytol for magnetic resonance imaging. Kidney Int. **92**, 47–66 (2017). https://doi.org/10.1016/j.kint.2016.12.037
56. E.D. Smolensky, H.-Y.E. Park, Y. Zhou, et al., Scaling laws at the nanosize: The effect of particle size and shape on the magnetism and relaxivity of iron oxide nanoparticle contrast agents. J. Mater. Chem. B **1**, 2818 (2013). https://doi.org/10.1039/c3tb00369h
57. A. Orza, H. Wu, Y. Xu, et al., One-step facile synthesis of highly magnetic and surface functionalized Iron oxide Nanorods for biomarker-targeted applications. ACS Appl. Mater. Interfaces **9**, 20719–20727 (2017). https://doi.org/10.1021/acsami.7b02575
58. J. Mohapatra, A. Mitra, H. Tyagi, et al., Iron oxide nanorods as high-performance magnetic resonance imaging contrast agents. Nanoscale **7**, 9174–9184 (2015). https://doi.org/10.1039/C5NR00055F
59. M.E. Materia, P. Guardia, A. Sathya, et al., Mesoscale assemblies of Iron oxide Nanocubes as heat mediators and image contrast agents. Langmuir **31**, 808–816 (2015). https://doi.org/10.1021/la503930s
60. Z. Zhao, Z. Zhou, J. Bao, et al., Octapod iron oxide nanoparticles as high-performance T2 contrast agents for magnetic resonance imaging. Nat. Commun. **4**, 2266 (2013). https://doi.org/10.1038/ncomms3266
61. Y. Bao, J.A. Sherwood, Z. Sun, Magnetic iron oxide nanoparticles as T1 contrast agents for magnetic resonance imaging. J. Mater. Chem. C **6**, 1280–1290 (2018). https://doi.org/10.1039/C7TC05854C
62. I. Fernández-Barahona, M. Muñoz-Hernando, J. Ruiz-Cabello, et al., Iron oxide nanoparticles: An alternative for positive contrast in magnetic resonance imaging. Inorganics **8**, 28 (2020). https://doi.org/10.3390/inorganics8040028
63. H. Wei, O.T. Bruns, M.G. Kaul, et al., Exceedingly small iron oxide nanoparticles as positive MRI contrast agents. Proc. Natl. Acad. Sci. **114**, 2325–2330 (2017). https://doi.org/10.1073/pnas.1620145114
64. T. Macher, J. Totenhagen, J. Sherwood, et al., Ultrathin Iron oxide Nanowhiskers as positive contrast agents for magnetic resonance imaging. Adv. Funct. Mater. **25**, 490–494 (2015). https://doi.org/10.1002/adfm.201403436
65. W. Yue, A.H. Hill, A. Harrison, W. Zhou, Mesoporous single-crystal Co3O4 templated by cage-containing mesoporous silica. Chem. Commun. (Camb.) **1**, 2518–2520 (2007). https://doi.org/10.1039/b700185a
66. Y. Yue, X. Wang, Nanoscale thermal probing. Nano Rev **3**, 11586 (2012). https://doi.org/10.3402/nano.v3i0.11586
67. Z. Zhou, D. Huang, J. Bao, et al., A synergistically enhanced T1-T2 dual-modal contrast agent. Adv. Mater. **24**, 6223–6228 (2012). https://doi.org/10.1002/adma.201203169
68. G. Vallejo-Fernandez, O. Whear, A.G. Roca, et al., Mechanisms of hyperthermia in magnetic nanoparticles. J. Phys. D. Appl. Phys. **46**, 312001 (2013). https://doi.org/10.1088/0022-3727/46/31/312001
69. S. Dutz, R. Hergt, Magnetic nanoparticle heating and heat transfer on a microscale: Basic principles, realities and physical limitations of hyperthermia for tumour therapy. Int. J. Hyperth. **29**, 790–800 (2013). https://doi.org/10.3109/02656736.2013.822993

70. A.E. Deatsch, B.A. Evans, Heating efficiency in magnetic nanoparticle hyperthermia. J. Magn. Magn. Mater. **354**, 163–172 (2014). https://doi.org/10.1016/j.jmmm.2013.11.006
71. M. Ma, Y. Wu, J. Zhou, et al., Size dependence of specific power absorption of Fe3O4 particles in AC magnetic field. J. Magn. Magn. Mater. **268**, 33–39 (2004). https://doi.org/10.1016/S0304-8853(03)00426-8
72. Z. Nemati, R. Das, J. Alonso, et al., Iron oxide Nanospheres and Nanocubes for magnetic hyperthermia therapy: A comparative study. J. Electron. Mater. **46**, 3764–3769 (2017). https://doi.org/10.1007/s11664-017-5347-6
73. D. Serantes, K. Simeonidis, M. Angelakeris, et al., Multiplying magnetic hyperthermia response by nanoparticle assembling. J. Phys. Chem. C **118**, 5927–5934 (2014). https://doi.org/10.1021/jp410717m
74. P. Guardia, R. Di Corato, L. Lartigue, et al., Water-soluble Iron oxide Nanocubes with high values of specific absorption rate for Cancer cell hyperthermia treatment. ACS Nano **6**, 3080–3091 (2012). https://doi.org/10.1021/nn2048137
75. P. Guardia, A. Riedinger, S. Nitti, et al., One pot synthesis of monodisperse water soluble iron oxide nanocrystals with high values of the specific absorption rate. J. Mater. Chem. B **2**, 4426 (2014). https://doi.org/10.1039/c4tb00061g
76. K. Mahmoudi, A. Bouras, D. Bozec, et al., Magnetic hyperthermia therapy for the treatment of glioblastoma: A review of the therapy's history, efficacy and application in humans. Int. J. Hyperth. **34**, 1316–1328 (2018). https://doi.org/10.1080/02656736.2018.1430867
77. M.V. Zyuzin, M. Cassani, M.J. Barthel, et al., Confining Iron oxide Nanocubes inside submicrometric cavities as a key strategy to preserve magnetic heat losses in an intracellular environment. ACS Appl. Mater. Interfaces **11**, 41957–41971 (2019). https://doi.org/10.1021/acsami.9b15501
78. J. Mohapatra, A. Mitra, M. Aslam, D. Bahadur, Octahedral-shaped Fe3O4 nanoparticles with enhanced specific absorption rate and R2 Relaxivity. IEEE Trans. Magn. **51**, 1–3 (2015). https://doi.org/10.1109/TMAG.2015.2439213
79. Y. Lv, Y. Yang, J. Fang, et al., Size dependent magnetic hyperthermia of octahedral Fe 3 O 4 nanoparticles. RSC Adv. **5**, 76764–76771 (2015). https://doi.org/10.1039/C5RA12558H
80. A. Wachowiak, Direct observation of internal spin structure of magnetic vortex cores. Science (80-) **298**, 577–580 (2002). https://doi.org/10.1126/science.1075302
81. M. Ma, Y. Zhang, Z. Guo, N. Gu, Facile synthesis of ultrathin magnetic iron oxide nanoplates by Schikorr reaction. Nanoscale Res. Lett. **8**, 16 (2013). https://doi.org/10.1186/1556-276X-8-16
82. S. Del Sol-Fernández, Y. Portilla-Tundidor, L. Gutiérrez, et al., Flower-like Mn-doped magnetic nanoparticles functionalized with α v β 3 -integrin-ligand to efficiently induce intracellular heat after alternating magnetic field exposition, triggering Glioma cell death. ACS Appl. Mater. Interfaces **11**, 26648–26663 (2019). https://doi.org/10.1021/acsami.9b08318
83. J. Estelrich, M. Busquets, Iron oxide nanoparticles in Photothermal therapy. Molecules **23**, 1567 (2018). https://doi.org/10.3390/molecules23071567
84. A. Espinosa, R. Di Corato, J. Kolosnjaj-Tabi, et al., Duality of Iron oxide nanoparticles in Cancer therapy: Amplification of heating efficiency by magnetic hyperthermia and Photothermal bimodal treatment. ACS Nano **10**, 2436–2446 (2016). https://doi.org/10.1021/acsnano.5b07249
85. A. Espinosa, J. Kolosnjaj-Tabi, A. Abou-Hassan, et al., Magnetic (hyper)Thermia or Photothermia? Progressive comparison of Iron oxide and gold nanoparticles heating in water, in cells, and in vivo. Adv. Funct. Mater. **28**, 1803660 (2018). https://doi.org/10.1002/adfm.201803660
86. D. Cheng, X. Li, G. Zhang, H. Shi, Morphological effect of oscillating magnetic nanoparticles in killing tumor cells. Nanoscale Res. Lett. **9**, 195 (2014). https://doi.org/10.1186/1556-276X-9-195
87. X. Yao, K. Sabyrov, T. Klein, et al., Evaluation of magnetic heating of asymmetric magnetite particles. J. Magn. Magn. Mater. **381**, 21–27 (2015). https://doi.org/10.1016/j.jmmm.2014.12.035

88. D.-H. Kim, E.A. Rozhkova, I.V. Ulasov, et al., Biofunctionalized magnetic-vortex microdiscs for targeted cancer-cell destruction. Nat. Mater. **9**, 165–171 (2010). https://doi.org/10.1038/nmat2591
89. M.P. Sharrock, Recent advances in metal particulate recording media: Toward the ultimate particle. IEEE Trans. Magn. **36**, 2420–2425 (2000). https://doi.org/10.1109/20.908453
90. M.P. Sharrock, Particulate magnetic recording media: A review. IEEE Trans. Magn. **25**, 4374–4389 (1989). https://doi.org/10.1109/20.45317
91. A. Berkowitz, Some materials considerations in particulate media. IEEE Trans. Magn. **22**, 466–471 (1986). https://doi.org/10.1109/TMAG.1986.1064462
92. A.E. Berkowitz, R.P. Goehner, E.L. Hall, P.J. Flanders, Microstructure, relaxation, and print-through in γ-Fe 2 O 3 particles. J. Appl. Phys. **57**, 3928–3930 (1985). https://doi.org/10.1063/1.334919
93. M. Stachen, M.P. Morales, M. Ocaña, C.J. Serna, Effect of precursor impurities on the magnetic properties of uniform γ-Fe2O3 ellipsoidal particles. Phys. Chem. Chem. Phys. **1**, 4465–4471 (1999). https://doi.org/10.1039/a904606b
94. H. Naono, R. Fujiwara, Micropore formation due to thermal decomposition of acicular microcrystals of α-FeOOH. J. Colloid Interface Sci. **73**, 406–415 (1980). https://doi.org/10.1016/0021-9797(80)90086-7
95. A. Corradi, S. Andress, J. French, et al., Magnetic properties of new (NP) hydrothermal particles. IEEE Trans. Magn. **20**, 33–38 (1984). https://doi.org/10.1109/TMAG.1984.1063007
96. M.P. Morales, S.A. Walton, L.S. Prichard, et al., Characterisation of advanced metal particle recording media pigments. J. Magn. Magn. Mater. **190**, 357–370 (1998). https://doi.org/10.1016/S0304-8853(98)00249-2
97. N.O. Nuñez, M.P. Morales, P. Tartaj, C.J. Serna, Preparation of high acicular and uniform goethite particles by a modified-carbonate route. J. Mater. Chem. **10**, 2561–2565 (2000). https://doi.org/10.1039/b005014h
98. R. Mendoza-Reséndez, M.P. Morales, C.J. Serna, Reduction mechanism of uniform iron oxide nanoparticles to metal used as recording media. Mater. Sci. Eng. C **23**, 1139–1142 (2003). https://doi.org/10.1016/j.msec.2003.09.126
99. T. Pradeep, Anshup, Noble metal nanoparticles for water purification: A critical review. Thin Solid Films **517**, 6441–6478 (2009). https://doi.org/10.1016/j.tsf.2009.03.195
100. A.S. Helal, E. Mazario, A. Mayoral, et al., Highly efficient and selective extraction of uranium from aqueous solution using a magnetic device: Succinyl-β-cyclodextrin-APTES@maghemite nanoparticles. Environ. Sci. Nano **5**, 158–168 (2018). https://doi.org/10.1039/C7EN00902J
101. M. Auffan, J. Rose, J.-Y. Bottero, et al., Towards a definition of inorganic nanoparticles from an environmental, health and safety perspective. Nat. Nanotechnol. **4**, 634–641 (2009). https://doi.org/10.1038/nnano.2009.242
102. M. Auffan, J. Rose, O. Proux, et al., Enhanced adsorption of arsenic onto Maghemites nanoparticles: As(III) as a probe of the surface structure and heterogeneity. Langmuir **24**, 3215–3222 (2008). https://doi.org/10.1021/la702998x
103. S. Brice-Profeta, M.-A. Arrio, E. Tronc, et al., Magnetic order in - nanoparticles: A XMCD study. J. Magn. Magn. Mater. **288**, 354–365 (2005). https://doi.org/10.1016/j.jmmm.2004.09.120
104. G.A. Waychunas, C.S. Kim, J.F. Banfield, Nanoparticulate Iron oxide minerals in soils and sediments: Unique properties and contaminant scavenging mechanisms. J. Nanopart. Res. **7**, 409–433 (2005). https://doi.org/10.1007/s11051-005-6931-x
105. M.S. Onyango, Y. Kojima, H. Matsuda, A. Ochieng, Adsorption kinetics of arsenic removal from groundwater by Iron-modified zeolite. J Chem Engineering Japan **36**, 1516–1522 (2003). https://doi.org/10.1252/jcej.36.1516
106. S.R. Chowdhury, E.K. Yanful, Arsenic and chromium removal by mixed magnetite–maghemite nanoparticles and the effect of phosphate on removal. J. Environ. Manag. **91**, 2238–2247 (2010). https://doi.org/10.1016/j.jenvman.2010.06.003

107. A. Khodabakhshi, M.M. Amin, M. Mozaffari, Synthesis of magnetite nanoparticles and evaluation of its efficiency for arsenic removal from simulated industrial waste water. Iran J Environ Heal Sci Eng **8**, 189–200 (2011)
108. L.-S. Zhong, J.-S. Hu, H.-P. Liang, et al., Self-assembled 3D flowerlike Iron oxide nanostructures and their application in water treatment. Adv. Mater. **18**, 2426–2431 (2006). https://doi.org/10.1002/adma.200600504
109. L. Balcells, C. Martínez-Boubeta, J. Cisneros-Fernández, et al., One-step route to Iron oxide hollow Nanocuboids by cluster condensation: Implementation in water remediation technology. ACS Appl. Mater. Interfaces **8**, 28599–28606 (2016). https://doi.org/10.1021/acsami.6b08709
110. M. Iram, C. Guo, Y. Guan, et al., Adsorption and magnetic removal of neutral red dye from aqueous solution using Fe3O4 hollow nanospheres. J. Hazard. Mater. **181**, 1039–1050 (2010). https://doi.org/10.1016/j.jhazmat.2010.05.119
111. C. Martinez-Boubeta, K. Simeonidis, *Magnetic Nanoparticles for Water Purification* (Nanoscale Materials in Water Purification. Elsevier, In, 2019), pp. 521–552
112. G.S. Parkinson, U. Diebold, J. Tang, L. Malkinski, Tailoring the Interface properties of magnetite for Spintronics. Adv Magn Mater, 61–88 (2012). https://doi.org/10.5772/39101
113. Z. Zhang, S. Satpathy, Electron states, magnetism, and the Verwey transition in magnetite. Phys. Rev. B **44**, 13319–13331 (1991). https://doi.org/10.1103/PhysRevB.44.13319
114. A. Mitra, B. Barick, J. Mohapatra, et al., Large tunneling magnetoresistance in octahedral Fe_3O_4 nanoparticles. AIP Adv. **6**, 055007 (2016). https://doi.org/10.1063/1.4948798
115. A. Mitra, J. Mohapatra, H. Sharma, et al., Controlled synthesis and enhanced tunnelling magnetoresistance in oriented Fe3O4 nanorod assemblies. J. Phys. D. Appl. Phys. **51**, 085002 (2018). https://doi.org/10.1088/1361-6463/aaa697
116. G. Sun, B. Dong, M. Cao, et al., Hierarchical dendrite-like magnetic materials of Fe 3 O 4 , γ-Fe 2 O 3 , and Fe with high performance of microwave absorption. Chem. Mater. **23**, 1587–1593 (2011). https://doi.org/10.1021/cm103441u
117. C.-L. Zhu, M.-L. Zhang, Y.-J. Qiao, et al., Fe 3 O 4 /TiO 2 Core/Shell nanotubes: Synthesis and magnetic and electromagnetic wave absorption characteristics. J. Phys. Chem. C **114**, 16229–16235 (2010). https://doi.org/10.1021/jp104445m
118. R.K. Walser, W. Win, P.M. Valanju, Shape-optimized ferromagnetic particles with maximum theoretical microwave susceptibility. IEEE Trans. Magn. **34**, 1390–1392 (1998). https://doi.org/10.1109/20.706558
119. L.L. Adebayo, H. Soleimani, N. Yahya, et al., Recent advances in the development OF Fe3O4-BASED microwave absorbing materials. Ceram. Int. **46**, 1249–1268 (2020). https://doi.org/10.1016/j.ceramint.2019.09.209
120. Y. Yang, M. Li, Y. Wu, et al., Size-dependent microwave absorption properties of Fe 3 O 4 nanodiscs. RSC Adv. **6**, 25444–25448 (2016). https://doi.org/10.1039/C5RA28035D
121. Y.J. Chen, P. Gao, C.L. Zhu, et al., Synthesis, magnetic and electromagnetic wave absorption properties of porous Fe_3O_4/Fe/SiO2 core/shell nanorods. J. Appl. Phys. **106**, 054303 (2009). https://doi.org/10.1063/1.3204958
122. X. Wang, F. Pan, Z. Xiang, et al., Magnetic vortex core-shell Fe3O4@C nanorings with enhanced microwave absorption performance. Carbon N Y **157**, 130–139 (2020). https://doi.org/10.1016/j.carbon.2019.10.030
123. X. Li, B. Zhang, C. Ju, et al., Morphology-controlled synthesis and electromagnetic properties of porous Fe 3 O 4 nanostructures from Iron Alkoxide precursors. J. Phys. Chem. C **115**, 12350–12357 (2011). https://doi.org/10.1021/jp203147q
124. X. Liu, Z. Zhong, Y. Tang, B. Liang, Review on the synthesis and applications of Fe_3O_4 Nanomaterials. J. Nanomater. **2013**, 1–7 (2013). https://doi.org/10.1155/2013/902538
125. J. Liu, Z. Wu, Q. Tian, et al., Shape-controlled iron oxide nanocrystals: Synthesis, magnetic properties and energy conversion applications. CrystEngComm **18**, 6303–6326 (2014). https://doi.org/10.1039/c6ce01307d

126. O. Delmer, P. Balaya, L. Kienle, J. Maier, Enhanced potential of amorphous electrode materials: Case study of RuO_2. Adv. Mater. **20**, 501–505 (2008). https://doi.org/10.1002/adma.200701349
127. J. Ma, X. Guo, Y. Yan, et al., FeO x -based materials for electrochemical energy storage. Adv. Sci. **5**, 1700986 (2018). https://doi.org/10.1002/advs.201700986
128. Z. Xiao, Y. Xia, Z. Ren, et al., Facile synthesis of single-crystalline mesoporous α-Fe2O3 and Fe3O4 nanorods as anode materials for lithium-ion batteries. J. Mater. Chem. **22**, 20566 (2012). https://doi.org/10.1039/c2jm34083f
129. S. Jin, H. Deng, D. Long, et al., Facile synthesis of hierarchically structured Fe_3O_4/carbon micro-flowers and their application to lithium-ion battery anodes. J. Power Sources **196**, 3887–3893 (2011). https://doi.org/10.1016/j.jpowsour.2010.12.078
130. Y. Zeng, R. Hao, B. Xing, et al., One-pot synthesis of Fe_3O_4 nanoprisms with controlled electrochemical properties. Chem. Commun. **46**, 3920 (2010). https://doi.org/10.1039/c0cc00246a
131. B. Koo, H. Xiong, M.D. Slater, et al., Hollow Iron oxide nanoparticles for application in Lithium ion batteries. Nano Lett. **12**, 2429–2435 (2012). https://doi.org/10.1021/nl3004286
132. H. Cao, R. Liang, D. Qian, et al., Serine-assisted synthesis of Superparamagnetic Fe3O4 Nanocubes for Lithium ion batteries. J. Phys. Chem. C **115**, 24688–24695 (2011). https://doi.org/10.1021/jp2096482
133. X.-L. Cheng, J.-S. Jiang, D.-M. Jiang, Z.-J. Zhao, Synthesis of rhombic dodecahedral Fe 3 O 4 Nanocrystals with exposed high-energy {110} facets and their peroxidase-like activity and Lithium storage properties. J. Phys. Chem. C **118**, 12588–12598 (2014). https://doi.org/10.1021/jp412661e